



## Article

# Beneficiation of Low-Grade Rare Earth Ore from Khalzan Buregtei Deposit (Mongolia) by Magnetic Separation

Ihwan Park <sup>1,\*</sup> , Yuki Kanazawa <sup>2</sup>, Naoya Sato <sup>2</sup>, Purevdelger Galtchandmani <sup>2</sup>, Manis Kumar Jha <sup>3</sup>, Carlito Baltazar Tabelin <sup>4</sup>, Sanghee Jeon <sup>1</sup>, Mayumi Ito <sup>1</sup> and Naoki Hiroyoshi <sup>1</sup> 

<sup>1</sup> Division of Sustainable Resources Engineering, Faculty of Engineering, Hokkaido University, Sapporo 060-8628, Japan; shjun1121@eng.hokudai.ac.jp (S.J.); itomayu@eng.hokudai.ac.jp (M.I.); hiroyosi@eng.hokudai.ac.jp (N.H.)

<sup>2</sup> Division of Sustainable Resources Engineering, Graduate School of Engineering, Hokkaido University, Sapporo 060-8628, Japan; kanazawa.yuki.c2@elms.hokudai.ac.jp (Y.K.); satonaoy@mmc.co.jp (N.S.); galtchandmani.p@bayanairag.com (P.G.)

<sup>3</sup> Metal Extraction and Recycling Division, CSIR-National Metallurgical Laboratory, Jamshedpur 831007, India; mkjha@nmlindia.org

<sup>4</sup> School of Minerals and Energy Resources Engineering, The University of New South Wales, Sydney, NSW 2052, Australia; c.tabelin@unsw.edu.au

\* Correspondence: i-park@eng.hokudai.ac.jp

**Abstract:** The global demand for rare earth elements (REEs) is expected to increase significantly because of their importance in renewable energy and clean storage technologies, which are critical for drastic carbon dioxide emission reduction to achieve a carbon-neutral society. REE ore deposits around the world are scarce and those that have been identified but remain unexploited need to be developed to supply future demands. In this study, the Khalzan Buregtei deposit located in western Mongolia was studied with the aim of upgrading low-grade REE ore via magnetic separation techniques. The total REE content in this ore was ~6720 ppm (~3540 ppm light REE (LREE) + ~3180 ppm heavy REE (HREE)) with bastnaesite, pyrochlore, synchysite, and columbite-(Fe) identified as the main REE-bearing minerals. As the particle size fraction decreased from  $-4.0 + 2.0$  mm to  $-0.5 + 0.1$  mm, the recovery by dry high-intensity magnetic separation (DHIMS) increased from 20% to 70% of total rare earth oxide (TREO) while the enrichment ratio reached 2.8 from 1.3. Although effective, gangue minerals such as quartz and aluminosilicates were recovered (~22%) due most likely to insufficient liberation. Meanwhile, the wet high-intensity magnetic separation (WHIMS) could produce a magnetic concentrate with TREO recovery of ~80% and enrichment ratio of 5.5 under the following conditions: particle size fraction,  $-106 + 75$   $\mu$ m; feed flow rate, 3.2 L/min; magnetic induction, 0.8 T. These results indicate that combining DHIMS and WHIMS to upgrade the low-grade REE ore from the Khalzan Buregtei deposit is an effective approach.

**Keywords:** rare earth elements; magnetic separation; upgradation; Khalzan Buregtei deposit



**Citation:** Park, I.; Kanazawa, Y.; Sato, N.; Galtchandmani, P.; Jha, M.K.; Tabelin, C.B.; Jeon, S.; Ito, M.; Hiroyoshi, N. Beneficiation of Low-Grade Rare Earth Ore from Khalzan Buregtei Deposit (Mongolia) by Magnetic Separation. *Minerals* **2021**, *11*, 1432. <https://doi.org/10.3390/min11121432>

Academic Editor: William Skinner

Received: 19 November 2021

Accepted: 15 December 2021

Published: 18 December 2021

**Publisher's Note:** MDPI stays neutral with regard to jurisdictional claims in published maps and institutional affiliations.



**Copyright:** © 2021 by the authors. Licensee MDPI, Basel, Switzerland. This article is an open access article distributed under the terms and conditions of the Creative Commons Attribution (CC BY) license (<https://creativecommons.org/licenses/by/4.0/>).

## 1. Introduction

Climate change is one of the most important and urgent issues faced by humanity this century that needs a solution [1–3]. The global mean temperature for 2020 was approximately  $1.2 \pm 0.1$  °C warmer than pre-industrial levels (i.e., the period 1850–1900) due to rising anthropogenic greenhouse gases (GHGs) in the atmosphere, in particular carbon dioxide (CO<sub>2</sub>) [4]. In 2015, the Paris Agreement was adopted by the 196 parties with the aim of limiting the global temperature rise to “well below 2 °C”, preferably to 1.5 °C, compared to pre-industrial levels [5]. In accordance with the Paris Agreement, 193 governments adopted the 17 sustainable development goals (SDGs), Goal 13 of which is “Climate Action” aiming at reducing CO<sub>2</sub> emission to combat climate change and achieve a carbon-neutral society by 2050 [6,7]. To become carbon-neutral, conventional fossil-fuel-

based electricity generation and transport technologies need to be replaced with renewable energy technologies as well as electric vehicles (EVs) [7–9].

However, low-carbon technologies are more intensive towards material, mineral and metal rather than conventional fossil-fuel-based technologies [7,8]. Among the materials for low-carbon technologies, rare earth elements (REEs)—a group of 17 elements consisting of lanthanides (lanthanum (La) to lutetium (Lu)) as well as scandium (Sc) and yttrium (Y)—are of great importance because significant quantities of REEs are utilized for manufacturing strong permanent magnet, a critical component used in generators for wind turbines and traction motors for EVs [8,10–12]. For example, 2 tons of REEs are required to build a 3 MW wind turbine, and the mass of REEs in a hybrid electric vehicle (HEV) with nickel-metal hydride (NiMH) batteries is approximately 3.5–4.5 kg [7,13–15]. Therefore, the stable supply of REEs for the next 20–30 years is important in the success of transitioning into a carbon-neutral society.

Although REEs are not scarce—the crustal abundance of REEs is about  $7 \times 10^{-5}$ – $4 \times 10^{-3}$  wt.%, more abundant than gold ( $5 \times 10^{-7}$  wt.%) and silver ( $1 \times 10^{-5}$  wt.%)—they are rarely found in deposits concentrated enough to be exploited economically [10,16]. The global production of REEs is dominated by only four countries: China (57.6%), USA (15.6%), Burma (12.3%), and Australia (7.0%) [17]. Due to their geographic production concentration, the REE supply chain is vulnerable to disruptions, and thus diversifying their supply sources is critical in maintaining a robust and stable supply chain.

According to the report by Bundesanstalt für Geowissenschaften und Rohstoffe (BGR) [18], Mongolia has a great potential to benefit from REEs as the country has four major REE deposits, named Khalzan Buregtei, Mushgai Khudag, Khotgor and Luginin Gol deposits (Figure 1a), with combined reserves of approximately 1.25 Mt REO. Among them, the Khalzan Buregtei deposit located in western Mongolia, approximately 50 km north of the city of Khovd, is considered the most important deposit because it is enriched in heavy REE (HREE), which is more expensive than light REE (LREE), as well as high field-strength elements (HFSEs) such as zirconium (Zr), niobium (Nb), tantalum (Ta), and yttrium (Y) [19–21]. Moreover, according to a report by the U.S. Geological Survey (USGS) [22], the global production of HREEs is lower than that of LREEs, which makes the development of appropriate beneficiation strategies for the Khalzan Buregtei deposit increasingly important.

The production of REE concentrates from ores has been conducted via the combination of gravity separation, magnetic separation, and flotation [16,23]. For example, shaking tables—one of the gravity separation techniques—either alone or in combination with flotation or magnetic separation were employed by a few hard rock REE beneficiation plants in Sichuan and Shandong in China, while Bayan Obo plant and some of the Sichuan operations use low-intensity magnetic separation (LIMS) to eliminate highly magnetic gangue minerals (e.g., magnetite ( $\text{Fe}_3\text{O}_4$ )) from the ground ore, two stages of wet high-intensity magnetic separation (WHIMS) to first recover hematite ( $\text{Fe}_2\text{O}_3$ ) and REE minerals from gangue minerals at higher magnetic field intensity and then separate hematite and REE minerals at lower magnetic field intensity, followed by flotation to further improve the grade of REE concentrates [24,25]. In summary, gravity and magnetic separation techniques are commonly adopted to preconcentrate REEs, while flotation is employed at the end of the process to produce saleable REE concentrates.

Beneficiation of the Khalzan Buregtei deposit has not been reported to date, so the appropriate preconcentration process should be established prior to investigating flotation. Between gravity and magnetic separation techniques, the former is less attractive for processing low-grade and fine-grained ores [16]; thus, this study aimed to investigate the applicability of dry/wet magnetic separation techniques for upgrading low-grade rare earth ore from the Khalzan Buregtei deposit. Specifically, the effects of particle size, feed flow rate and magnetic induction, the main factors affecting magnetic separation, on total rare earth oxide (TREO) recovery/grade were examined.

## 2. Materials and Methods

### 2.1. Rare Earth Ore Sample

The rare earth ore sample used in this study was obtained from the Khalzan Buregtei deposit, Khovd, Mongolia. As shown in Figure 1b, this deposit has multiple geological units consisting of seven intrusive phases, and among them, the 5th (orange area) and 7th (blue-gray area) phases are mineralized rocks forming the rare-metal peralkaline granitic ore [26]. The mineral compositions of the 5th and 7th phases are very similar, but the former is recognized as having coarse- and medium-grained rare-metal peralkaline granite while the latter consists of fine- and medium-grained miarolitic rare-metal peralkaline granite [26]. In this study, the 5th phase ore was used. The ore sample was crushed by a jaw crusher (BB 51, Retsch Inc. Haan, Germany), ground with a ball mill, and screened to obtain the predetermined size fractions. For the chemical and mineralogical analyses of the ore, the sample was further ground to  $<50\ \mu\text{m}$  using an agate mortar and pestle and then analyzed by X-ray fluorescence spectroscopy (XRF, EDXL300, Rigaku Corporation, Tokyo, Japan) and X-ray powder diffraction (XRD, MultiFlex, Rigaku Corporation, Tokyo, Japan). The XRD pattern was analyzed using the Match!® software (Crystal Impact GbR, Bonn, Germany). Thin sections of the ore were also prepared and analyzed by scanning electron microscopy with energy-dispersive X-ray spectroscopy (SEM-EDS, JSM-IT200, JEOL Ltd., Tokyo, Japan).

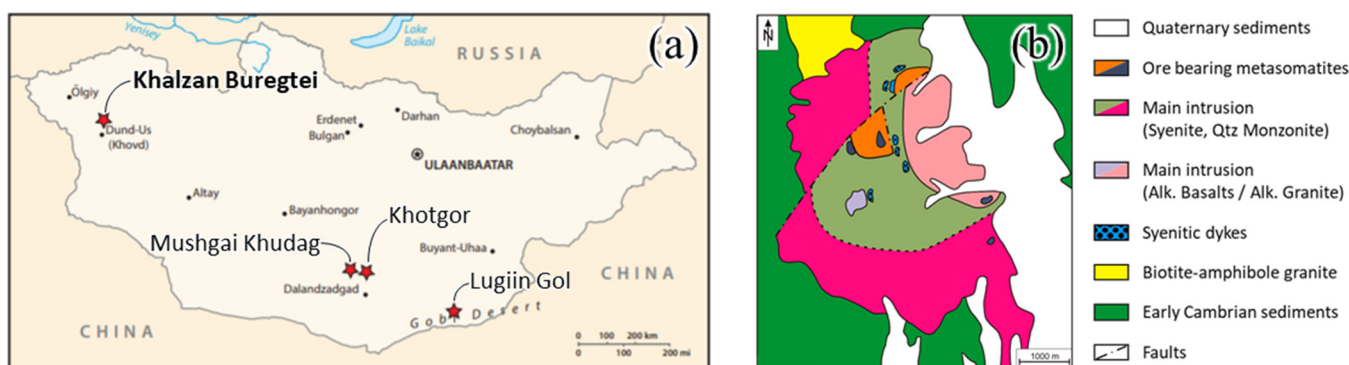


**Figure 1.** (a) A schematic location map of major Mongolian REE deposits (reprinted with permission from Muff and Tamiraa [18]), and (b) a geological sketch map of the Khalzan Buregtei deposit (reprinted with permission from Gronen et al. [20]).

### 2.2. Dry High-Intensity Magnetic Separation

Dry magnetic separation was conducted to recover rare earth minerals from coarse size fractions ( $-4 + 2$ ,  $-2 + 0.5$ , and  $-0.5 + 0.1\ \text{mm}$ ) of the crushed ore sample. A dry high-intensity rare earth roll separator (RE6D06W-1, Eriez Magnetics Co. Ltd., Chiba, Japan), consisting of a rare earth roll (75.4 mm diameter  $\times$  150 mm width) and an idler roll enveloped with a 0.25 mm thickness Kevlar belt, was used (Figure 2a). The sample was fed to the separator through the vibratory feeder, and magnetic separation was conducted with a belt speed of 8.7 m/min and magnetic field intensity of 1.2 T. The recovered non-magnetic fractions were re-circulated back to the separator to improve REE recovery, which was repeated twice (total pass = 3). The final magnetic and non-magnetic fractions were ground to  $<50\ \mu\text{m}$  and analyzed by XRF.

### 2.3. Wet High-Intensity Magnetic Separation

A dry magnetic separator is typically inefficient in processing fine-grained particles due to the influence of airflow, particle-particle adhesion and particle-rotor adhesion, so a wet high-intensity magnetic separator (WHIMS, L-4, Eriez Co. Ltd., Chiba, Japan) (Figure 2b) was adopted for recovering REEs from fine fractions ( $-212 + 106$ ,  $-106 + 75$ , and  $-75\ \mu\text{m}$ ) [27]. In the separation cell, 16 pieces of fine, expanded metal matrix (opening size: 2 mm  $\times$  5 mm) were placed to increase the number of high field gradient sites where magnetic particles could be collected. For each test, 30 g of sample was suspended in

600 mL of deionized (DI) water with 250 mg/L of sodium hexametaphosphate (SHMP,  $(\text{NaPO}_3)_6$ , Wako Pure Chemical Industries, Ltd., Osaka, Japan) as a dispersant, and then dispersed for 3 min with an ultrasonicator (W-113, Honda Electronics Co., Ltd., Toyohashi, Japan). Afterwards, a predetermined magnetic induction (0.2–1.0 T) was applied to the separation cell, and then the pulp was fed into the funnel placed on the top of WHIMS at a flow rate of 0–5.8 L/min, which was adjusted by controlling the discharge valve. A flow rate of 0 L/min means the feed was retained in the separation cell for 3 min by fully closing the discharge valve. When the slurry was entirely passed through the WHIMS, 1 L of DI water was introduced to wash the collected magnetic particles, which minimize the entrainment of non-magnetic particles in the magnetic concentrate. The recovered non-magnetic fraction was re-circulated back to the WHIMS to improve REE recovery, which was repeated twice (total pass = 3). The final magnetic and non-magnetic fractions were dried at 105 °C for 24 h, ground to <50  $\mu\text{m}$ , and analyzed by XRF. Some of the experiments were done in triplicate, and the relative standard deviations were <5%.

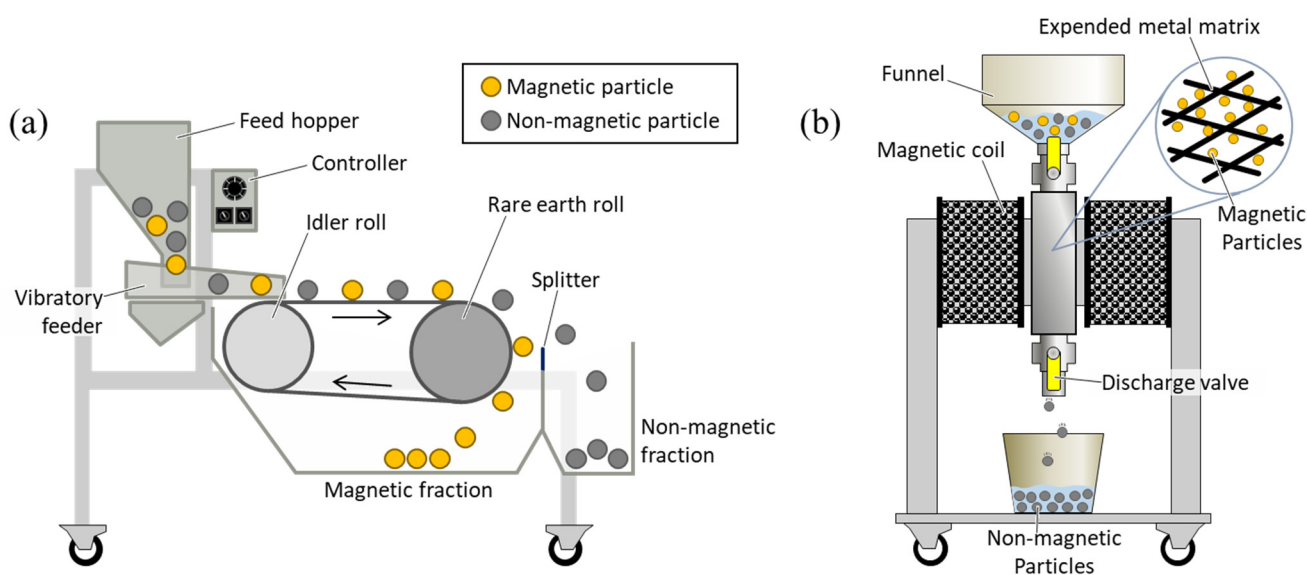


**Figure 2.** Schematic diagrams of (a) dry high-intensity magnetic separator and (b) wet high-intensity magnetic separator.

### 3. Results and Discussion

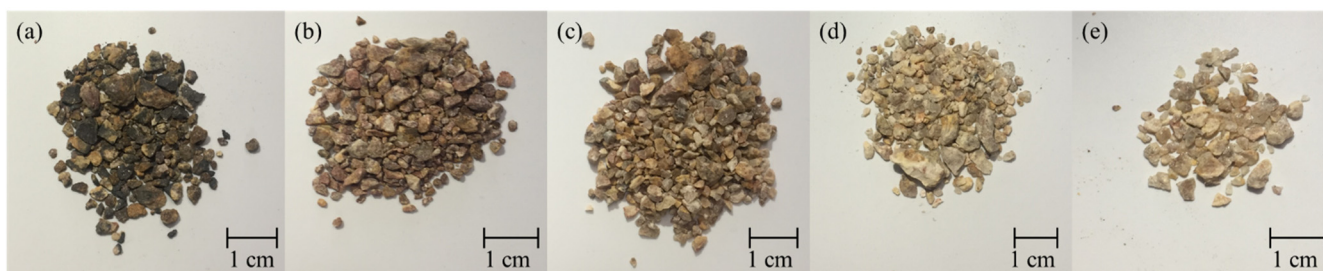
#### 3.1. Characterization of REE-Bearing Ore of Khalzan Buregtei Deposit, Mongolia

Table 1 shows the chemical composition of the ore sample of the Khalzan Buregtei deposit. As can be seen, the sample is rich in Si (69.0%) and Al (16.1%), while Fe, K, Zr, Ca, Nb, Ti, and Na are contained in the sample as minor non-REE constituents in the ranges of 0.05–4.1%. The TREO content in the sample is 6720 ppm, and LREE (La to Eu) and HREE (Gd to Lu plus Y) contents are 3540 and 3180 ppm, respectively.

**Table 1.** Elemental composition of REE-bearing sample from the Khalzan Buregtei deposit, Mongolia.

Non-REE	Content (%)	REE	Content (ppm)
SiO <sub>2</sub>	69.0 ± 2.2	La <sub>2</sub> O <sub>3</sub>	548 ± 184
Al <sub>2</sub> O <sub>3</sub>	16.1 ± 0.8	CeO <sub>2</sub>	1376 ± 460
Fe <sub>2</sub> O <sub>3</sub>	4.1 ± 0.79	Eu <sub>2</sub> O <sub>3</sub>	1004 ± 493
K <sub>2</sub> O	3.5 ± 0.42	Gd <sub>2</sub> O <sub>3</sub>	391 ± 63
ZrO <sub>2</sub>	3.6 ± 0.63	Y <sub>2</sub> O <sub>3</sub>	1809 ± 339
CaO	1.3 ± 0.12	Dy <sub>2</sub> O <sub>3</sub>	525 ± 117
Nb <sub>2</sub> O <sub>5</sub>	0.4 ± 0.11	Er <sub>2</sub> O <sub>3</sub>	73 ± 21
TiO <sub>2</sub>	0.4 ± 0.07	Yb <sub>2</sub> O <sub>3</sub>	181 ± 36
Na <sub>2</sub> O	0.05 ± 0.12	Other REEs	813 ± 282
Others	0.8 ± 0.18	TREO	6720 ± 1257

As shown in Figure 3, mineral particles were sorted based on the color to further identify the distribution of REEs; that is, mineral particles were divided into five groups (e.g., black, brown, brownish yellow, yellow, and transparent), and the chemical composition of each group was given in Table 2. The TREO contents were found to decrease in the following order: black (8640 ppm) > brown (7930 ppm) > brownish yellow (3030 ppm) > yellow (1690 ppm) > transparent (560 ppm). In the case of non-REE components, the contents of Fe, Zr, and Nb were high in black and brown groups where TREO contents were highest, which implies that REEs are most likely incorporated in Fe-, Zr-, and/or Nb-bearing minerals. Meanwhile, the major constituent, Si, was inversely proportional to TREO contents; that is, Si content increased from 66.2% in the black group to 93.9% in the transparent group, indicating that particles in the transparent group are most likely quartz (SiO<sub>2</sub>).



**Figure 3.** Photographs of samples sorted based on color: (a) black, (b) brown, (c) brownish yellow, (d) yellow, and (e) transparent particles.

**Table 2.** Elemental composition of samples sorted based on color.

Elements		(a)	(b)	(c)	(d)	(e)
Non-REE (%)	SiO <sub>2</sub>	66.2 ± 0.1	68.6 ± 0.4	71.2 ± 0.1	75.6 ± 0.2	93.9 ± 0.0
	Al <sub>2</sub> O <sub>3</sub>	14.4 ± 0.1	15.4 ± 0.5	18.6 ± 0.1	14.3 ± 0.1	4.0 ± 0.01
	Fe <sub>2</sub> O <sub>3</sub>	8.2 ± 0.03	4.6 ± 0.03	1.3 ± 0.01	2.0 ± 0.00	0.4 ± 0.00
	K <sub>2</sub> O	2.8 ± 0.12	3.1 ± 0.04	6.8 ± 0.03	2.7 ± 0.10	0.8 ± 0.01
	ZrO <sub>2</sub>	3.1 ± 0.03	5.9 ± 0.09	0.9 ± 0.01	0.7 ± 0.01	0.6 ± 0.00
	CaO	1.6 ± 0.01	2.3 ± 0.01	0.1 ± 0.01	1.1 ± 0.01	0.3 ± 0.01
	Nb <sub>2</sub> O <sub>5</sub>	0.4 ± 0.00	0.3 ± 0.00	0.2 ± 0.00	0.2 ± 0.00	n.d.*
REE (ppm)	La <sub>2</sub> O <sub>3</sub>	150 ± 9	240 ± 8	140 ± 6	160 ± 8	n.d.*
	CeO <sub>2</sub>	490 ± 38	660 ± 17	270 ± 15	460 ± 7	70 ± 8
	Nd <sub>2</sub> O <sub>3</sub>	n.d.*	420 ± 0	n.d.*	n.d.*	n.d.*
	Sm <sub>2</sub> O <sub>3</sub>	n.d.*	280 ± 9	510 ± 79	n.d.*	50 ± 9
	Eu <sub>2</sub> O <sub>3</sub>	3310 ± 650	1360 ± 910	420 ± 148	n.d.*	130 ± 57
	Gd <sub>2</sub> O <sub>3</sub>	1290 ± 50	n.d.*	120 ± 20	570 ± 30	n.d.*
	Y <sub>2</sub> O <sub>3</sub>	1960 ± 10	2960 ± 40	1020 ± 10	210 ± 2	160 ± 1
	Dy <sub>2</sub> O <sub>3</sub>	1090 ± 92	1410 ± 70	200 ± 17	230 ± 28	60 ± 7
	Er <sub>2</sub> O <sub>3</sub>	n.d.*	40 ± 47	100 ± 13	n.d.*	20 ± 8
	Tm <sub>2</sub> O <sub>3</sub>	230 ± 93	460 ± 30	150 ± 13	60 ± 20	40 ± 9
	Yb <sub>2</sub> O <sub>3</sub>	120 ± 50	100 ± 18	100 ± 4	n.d.*	30 ± 6
TREO	8640 ± 526	7930 ± 183	3030 ± 213	1690 ± 26	560 ± 33	

\* Abbreviation: n.d., not detected.

The mineralogical composition of the sample was determined by XRD (Figure 4). As shown in the XRD pattern, quartz and aluminosilicates (e.g., albite (NaAlSi<sub>3</sub>O<sub>8</sub>) and microcline (KAlSi<sub>3</sub>O<sub>8</sub>)) were identified as the main gangue minerals in the sample, which is consistent with the XRF result (Table 1). Meanwhile, hematite (Fe<sub>2</sub>O<sub>3</sub>), aegirine (NaFe<sup>3+</sup>Si<sub>2</sub>O<sub>6</sub>), arfvedsonite (NaNa<sub>2</sub>(Fe<sup>2+</sup><sub>4</sub>Fe<sup>3+</sup>)Si<sub>8</sub>O<sub>22</sub>(OH)<sub>2</sub>), zircon (ZrSiO<sub>4</sub>), and columbite-(Fe) (FeNb<sub>2</sub>O<sub>6</sub>) were minerals containing minor non-REE constituents (e.g., Fe, Zr, and Nb). Due to the low grade of REEs in the sample, REE-bearing minerals were not detected in the XRD pattern, thus, SEM-EDS analysis of thin sections was conducted to clarify the types of REE-bearing

minerals in the sample. As illustrated in Figure 5, the major REE-bearing minerals were identified to be bastnaesite-(Ce) ( $\text{Ce}(\text{CO}_3)\text{F}$ ) and pyrochlore ( $(\text{Na,Ca,REE})_2\text{Nb}_2\text{O}_6(\text{OH,F})$ ), which are locked within the quartz/albite matrix. Moreover, synchysite ( $\text{Ca}(\text{REE})(\text{CO}_3)_2\text{F}$ ) and columbite-(Fe) were found to be REE-bearing minerals (Figure S1). Zircon has been reported to incorporate REEs into its structure [20,28,29], but REE signals were not detected on zircon (Figure S1). The grain sizes of REE-carbonates (e.g. bastnaesite and synchysite) and pyrochlore varied from 10 to 154  $\mu\text{m}$  and 10 to 243  $\mu\text{m}$ , respectively (Figures 4 and S1).

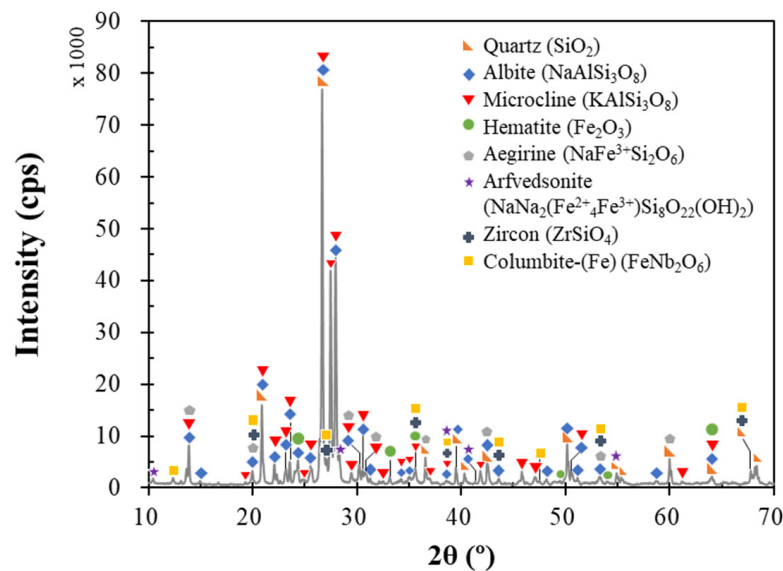


Figure 4. XRD pattern of the REE-bearing sample from the Khalzan Buregtei deposit, Mongolia.

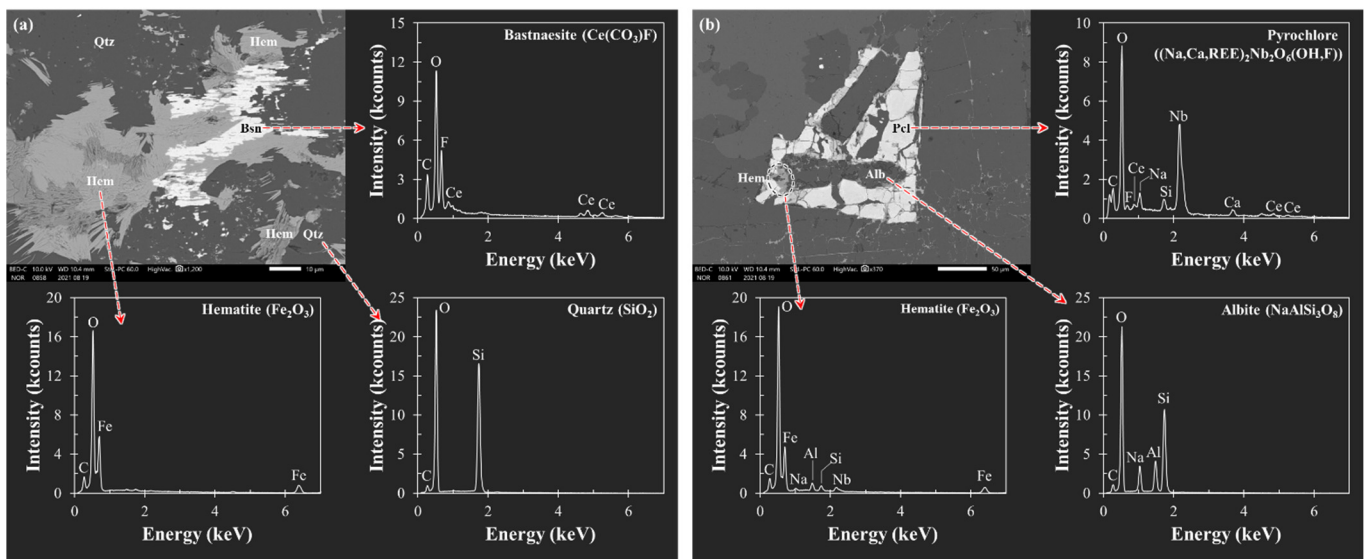


Figure 5. Back-scattered electron (BSE) images and EDS point analyses of (a) bastnaesite-hematite-quartz and (b) pyrochlore-hematite-albite ores in the sample. Note: Bsn, bastnaesite; Hem, hematite; Qtz, quartz; Pcl, pyrochlore; Alb, albite.

### 3.2. Dry High-Intensity Magnetic Separation

Upgrading REO from coarse size fractions ( $-4 + 2$  mm,  $-2 + 0.5$  mm, and  $-0.5 + 0.1$  mm) was carried out using dry high-intensity magnetic separation. Figure 6 shows the recovery of TREO, Fe and Si, their enrichment ratios, and Newton's efficiency ( $\eta$ ), which were calculated according to the following equations:

$$\text{Recovery (\%)} = \frac{C_c}{F_f} \times 100\%, \quad (1)$$

$$\text{Enrichment ratio} = \frac{c}{f}, \quad (2)$$

$$\eta(\%) = R_c - (100 - R_t), \quad (3)$$

where F and C are the weights of feed and concentrate, f and c are the grades of elements (REEs, Fe, and Si) in feed and concentrate, and  $R_c$  and  $R_t$  are the recoveries of REEs in the concentrate and gangue minerals in the tailing.

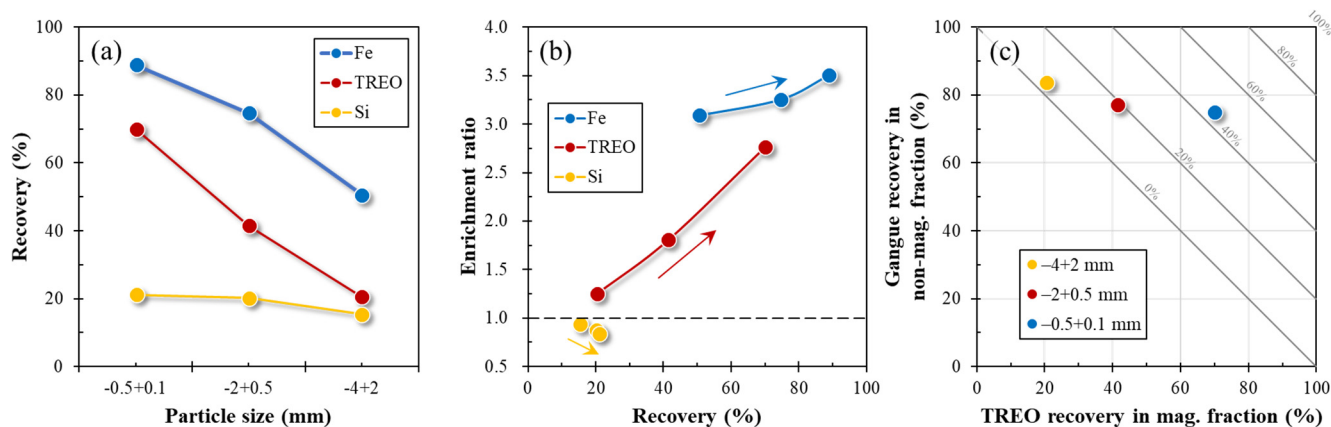


**Figure 6.** Effect of particle size on (a) the recovery of TREO, Fe, and Si from REE ore, (b) enrichment ratios of TREO, Fe, and Si as a function of recovery, and (c) relationship between TREO recovery in magnetic fraction and gangue recovery in non-magnetic fraction. Note: The arrows in Figure 6b indicate the particle size decreasing from  $-4 + 2$  mm to  $-0.5 + 0.1$  mm.

As shown in Figure 6a, TREO recovery increased from 20% to 70% with decreasing particle size. The Fe recovery also showed the same trend as that of TREO, but iron-bearing minerals were more strongly attracted by the rare earth roll magnet than REO; that is, Fe recovery increased from 50% to 89% as particle size decreased. These results are to be expected because of the moderate to strong attraction of iron-bearing minerals/materials to a magnetic field [30–32]. These results indicate that the smaller the particles, the greater the liberation of REE- and Fe-minerals locked within the quartz/albite matrix, and thus their recoveries could be improved. Although TREO recovery increased with decreasing particle size, Si recovery was almost kept constant (15%–20%) regardless of particle size, indicating that gangue minerals were not sufficiently separated from REE- and/or Fe-minerals even in the size fraction of  $-0.5 + 0.1$  mm. As the recoveries of TREO and Fe were selectively increased while Si recovery was kept constant, the grades of TREO and Fe were enriched by 1.3–2.8 and 3.1–3.5 times, respectively (Figure 6b). Moreover, the separation efficiency of TREO from gangue minerals was remarkably increased from ~4.2% to ~45% with decreasing particle size (Figure 6c).

### 3.3. Wet High-Intensity Magnetic Separation

Although the dry high-intensity magnetic separator (DHIMS) concentrated REO by 2.8-fold, approximately 30% of REO was lost to the non-magnetic fraction due most likely to insufficient liberation. To improve the liberation of REO from the gangue minerals, finer grinding is required; however, particles finer than 100  $\mu$ m are difficult to recover by

DHIMS [27,33,34]. Because of this, WHIMS—well-known for its ability to recover fine weakly magnetic minerals [33]—was employed. Figure 7 compares the performance of DHIMS (for  $-0.5 + 0.1$  mm fraction) and WHIMS (for  $-106 + 75$   $\mu\text{m}$  fraction) on TREO recovery and the separation efficiency. Between the two, WHIMS showed better TREO recovery ( $\sim 82\%$ ) and separation efficiency ( $\sim 60\%$ ) than DHIMS (i.e., TREO recovery,  $\sim 70\%$ ; separation efficiency,  $\sim 45\%$ ). As the processing of finer particles via WHIMS showed promising results for improving TREO recovery as well as the separation efficiency of REO from gangue minerals compared with DHIMS, it was further investigated under various conditions (e.g., particle size, feed flow rate, and magnetic induction strength).

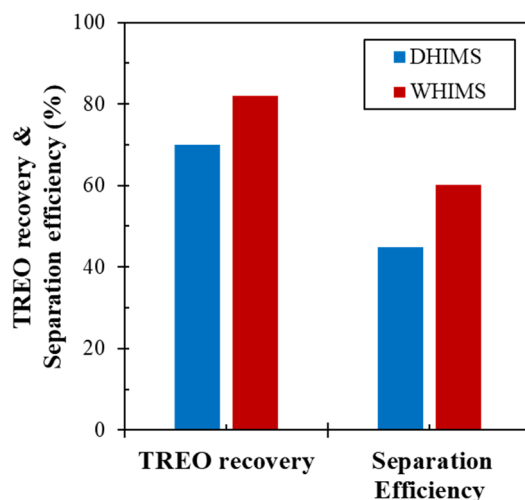


Figure 7. Comparison of TREO recovery and separation efficiency by DHIMS and WHIMS.

### 3.3.1. Effect of Particle Size

Figure 8a shows the effect of particle size on the recovery of TREO, Fe, and Si operated at a magnetic induction of 1 T and a feed flow rate of 3.2 L/min. The recoveries of TREO and Fe were 79–88% and 89–94%, respectively, both of which slightly decreased with decreasing particle size. The magnetic force acting on a particle is given by the following equation [33]:

$$\vec{F}_m = \frac{\kappa}{\mu_0} V |\mathbf{B} \text{grad} \mathbf{B}|, \quad (4)$$

where  $\kappa$  is the volume magnetic susceptibility,  $\mu_0$  is the permeability of free space (numerically equal to  $4\pi \times 10^{-7} \text{ Hm}^{-1}$ ),  $V$  is the volume of the particle, and  $\mathbf{B}$  and  $\text{grad} \mathbf{B}$  are the magnetic induction and its gradient, respectively. As can be seen in Equation (4),  $F_m$  is proportional to the volume of the particle, which indicates that the recoveries of TREO and Fe were decreased because of the decreased  $F_m$  when particle size is reduced.

It is important to note that although the decrease in particle size slightly reduced the recovery of TREO, it was particularly beneficial in reducing the recovery of the major gangue minerals (e.g., quartz and other silicate minerals); that is, Si recovery was  $\sim 34\%$  in the  $-212 + 106$   $\mu\text{m}$  size fraction but decreased to  $\sim 15\%$  when particle size became  $<106$   $\mu\text{m}$ . Reduction of Si recovery from  $\sim 34\%$  to  $\sim 15\%$  translated into a better enrichment ratio of TREO from 2.4 to 3.8–3.9 (Figure 8b). Similarly, Fe enrichment ratio increased from 2.5 to 4.3–4.4 as particle size decreased, whereas Si enrichment ratio decreased from 0.9 to 0.7. As shown in Figure 8c, the separation efficiencies of TREO from gangue minerals at various particle sizes are in the following order:  $-106 + 75$   $\mu\text{m}$  (60%)  $\approx$   $-75$   $\mu\text{m}$  (59%)  $>$   $-212 + 106$   $\mu\text{m}$  (51%). These results indicate that the  $-106 + 75$   $\mu\text{m}$  size fraction showed better REO upgrading and recovery compared with the other size fractions, so the particle size of the sample was fixed to  $-106 + 75$   $\mu\text{m}$  for the following experiments.



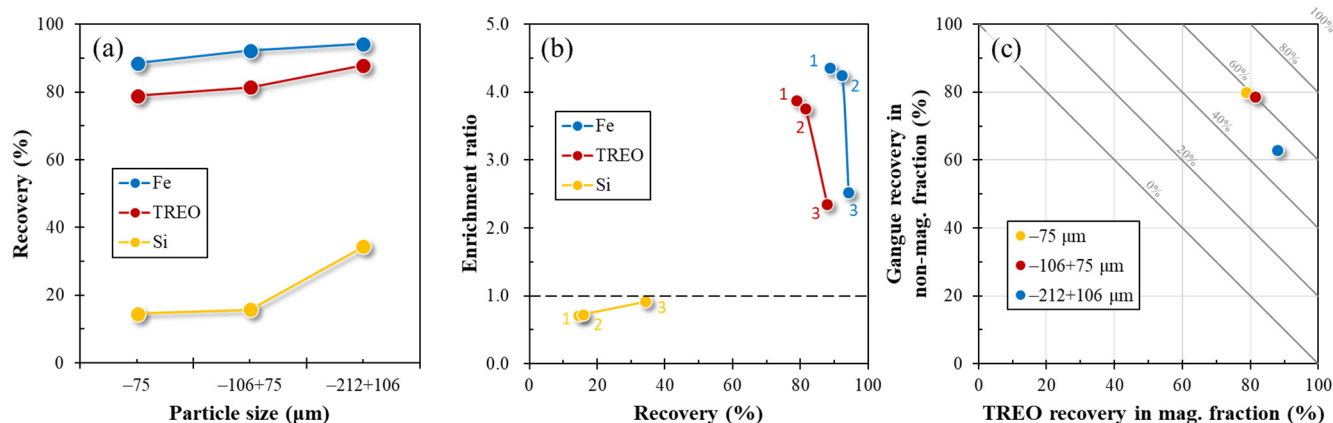


**Figure 8.** Effect of particle size on (a) the recovery of TREO, Fe, and Si from REE ore, (b) enrichment ratio as a function of recovery, and (c) relationship between TREO recovery in magnetic fraction and gangue recovery in non-magnetic fraction. Note: The numbers in Figure 8b denote that particle size (1: -75 μm, 2: -106 + 75 μm, 3: -212 + 106 μm).

### 3.3.2. Effect of Feed Flow Rate

The movement of mineral particles in the separation chamber of WHIMS is influenced by not only the magnetic force but also the fluid resistance (drag) force ( $F_d$ , Equation (5)) and the gravitational force ( $F_g$ , Equation (6)). The latter two physical forces acting on mineral particles are known as competing forces [33]:

$$\vec{F}_d = 3\pi\eta d \left( \vec{v}(\vec{r}) - \frac{d\vec{r}}{dt} \right), \quad (5)$$

$$\vec{F}_g = \frac{1}{6}\pi(\rho_p - \rho_f)d^3\vec{g}, \quad (6)$$

where  $\eta$  is the dynamic viscosity of the fluid,  $d$  is the particle diameter,  $v(r)$  is the velocity of the particle at position  $r$ ,  $dr/dt$  is the velocity of the fluid,  $\rho_p$  and  $\rho_f$  are the densities of the particle and the fluid medium, and  $g$  is the gravitational acceleration. For a magnetic particle to be retained by the magnetized matrix, the magnetic force has to overcome all other physical forces (i.e.,  $F_m \gg F_d + F_g$ ) [35]. As illustrated in Equation (5), the drag force is strongly influenced by the feed flow rate. At a low feed flow rate, retention of magnetic minerals by the magnetized matrix increases as the drag force is weakened, but the entrainment of gangue minerals is also increased, leading to lowering of the grade of products. At a high feed flow rate, on the other hand, the recovery of magnetic minerals, as well as the entrainment of gangue minerals, are both decreased. Thus, the operation at the appropriate feed flow rate is of importance for the recovery/grade of TREO.

Figure 9a shows the effect of feed flow rate on the recovery of TREO, Fe, and Si at a magnetic induction of 1 T. The recovery of magnetic minerals (i.e., REO and iron-minerals) slightly increased as the feed flow rate decreased; that is, the recoveries of TREO and Fe increased from 73% to 88% and from 87% to 98%, respectively. It is important to note that the recovery of Si was less than 23% at the range of 1.6–5.8 L/min but significantly increased to 49% at a feed flow rate of 0 L/min. This indicates that the lowering of the feed flow rate enhanced the recovery of not only REO but also gangue minerals. As displayed in Figure 9b, the enrichment ratios of magnetic minerals peaked at 3.2 L/min but decreased at feed flow rates of <3.2 L/min. Moreover, the separation efficiencies of TREO from gangue minerals at various feed flow rates (Figure 9c) are in the following order: 3.2 L/min (60%) > 1.6 L/min (57%) > 5.8 L/min (51%) > 0 L/min (41%). Thus, 3.2 L/min is the most effective feed flow rate for upgrading REO from the ore in this study.

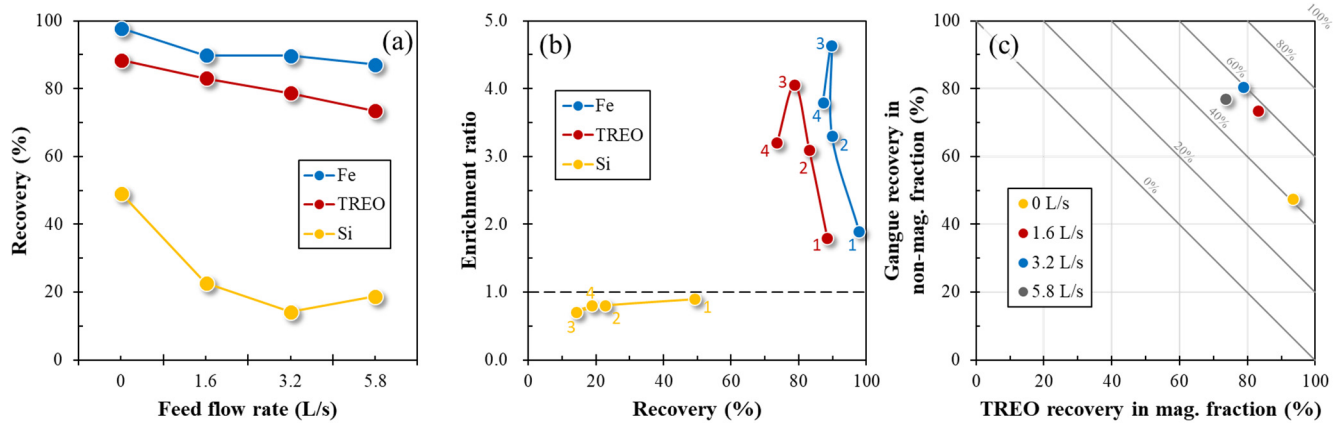


**Figure 9.** Effect of feed flow rate on (a) the recovery of TREO, Fe, and Si from REE ore, (b) enrichment ratio as a function of recovery, and (c) relationship between TREO recovery in magnetic fraction and gangue recovery in non-magnetic fraction. Note: The numbers in Figure 9b denote that the feed flow rate (1: 0 L/s, 2: 1.6 L/s, 3: 3.2 L/s, 4: 5.8 L/s).

### 3.3.3. Effect of Magnetic Induction

Magnetic induction is one of the most important factors controlling the recovery of target minerals during magnetic separation. As explained by Equation (4), the magnetic force ( $F_m$ ) is proportional to the magnetic induction, which means that the recovery of magnetic minerals is promoted at higher magnetic induction. As illustrated in Figure 10a, magnetic induction has a significant effect on the recovery of TREO. At 0.4–0.6 T, the recovery of TREO was 66–67% that increased to 77–79% at higher magnetic induction (0.8–1.0 T). In contrast, the recovery of iron minerals was almost constant (84–90%) irrespective of magnetic induction. This difference could be explained by the higher magnetic susceptibilities of iron minerals (e.g., hematite,  $0.4\text{--}7.0 \times 10^{-3}$ ; magnetite,  $3.0 \times 10^0$ ) compared with REE minerals (e.g., bastnaesite,  $0.2 \times 10^{-3}$ ) [36,37], which allow the former to be collected in the magnetized matrix even at a low magnetic induction. The recovery of Si was low (5–8%) irrespective of magnetic induction. As shown in Figure 10b, the enrichment ratio of TREO increased from 4.9 to 5.5 as magnetic induction increased to 0.8 T but slightly decreased to 5.3 at 1.0 T. Moreover, the separation efficiency was ~64% at 0.8–1.0 T and 53–54% at 0.4–0.6 T (Figure 10c). This indicates a magnetic induction of 0.8 T was the most effective in upgrading REO from the ore; that is, the grade of TREO could be enriched by approximately 5.5-fold (i.e., feed: 7240 ppm, magnetic concentrate: 39,800 ppm).

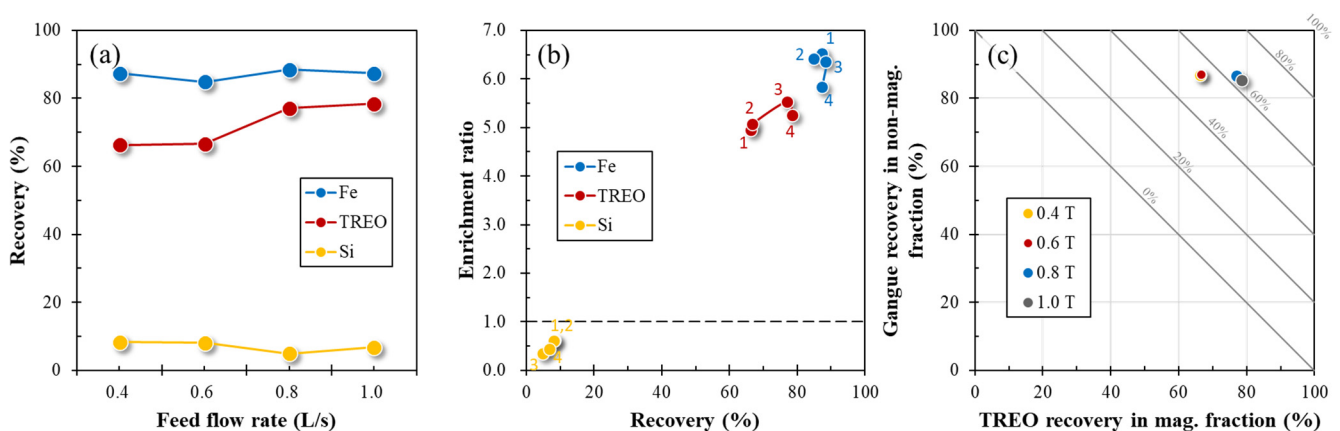


**Figure 10.** Effect of magnetic induction on (a) the recovery of TREO, Fe, and Si from REE ore, (b) enrichment ratio as a function of recovery, and (c) relationship between TREO recovery in magnetic fraction and gangue recovery in non-magnetic fraction. Note: The numbers in Figure 10b denote that the magnetic induction (1: 0.4 T, 2: 0.6 T, 3: 0.8 T, 4: 1.0 T).

#### 4. Conclusions

This study investigated the dry/wet magnetic separation for upgrading REO from the Khalzan Buregtei ore deposit, Mongolia. The ore used in this study has a low total REE content (~6720 ppm) but contains a relatively high content of HREE (~3180 ppm). The ore is predominantly composed of quartz and aluminosilicate minerals (e.g., albite and microcline) with minor amounts of Fe-, Zr-, and Nb-bearing minerals (e.g., hematite, aegirine, arfvedsonite, zircon, and columbite-(Fe)) and trace amounts of REE-bearing minerals (e.g., bastnaesite, pyrochlore, and synchysite). The dry high-intensity magnetic separation of  $-0.5 + 0.1$  mm size fraction concentrated REO by 2.8-fold with 70% recovery. Compared with DHIMS, the multistage WHIMS showed exceptional results (i.e., TREO recovery, ~80%; enrichment ratio, 5.5) under the following conditions: particle size,  $-106 + 75$   $\mu\text{m}$ ; feed flow rate, 3.2 L/min; magnetic induction, 0.8 T. Based on the findings of this study, it has been confirmed that combining dry and wet magnetic separation is an effective pre-concentration stage where the grade of TREO could be enriched by more than 5-fold (~39,800 ppm) and ~90% of gangue minerals are removed from magnetic concentrates. To further upgrade REO from magnetic concentrates, finer grinding ( $<75$   $\mu\text{m}$ ) followed by froth flotation is recommended.

**Supplementary Materials:** The following are available online at <https://www.mdpi.com/article/10.3390/min11121432/s1>, Figure S1: Back-scattered electron (BSE) images and EDS point analyses of REE ore thin-section.

**Author Contributions:** Conceptualization, I.P., M.I. and N.H.; methodology, I.P. and S.J.; investigation, Y.K., N.S. and P.G.; resources, P.G.; data curation, I.P. and Y.K.; writing—original draft preparation, I.P.; writing—review and editing, I.P., S.J., M.I., M.K.J., C.B.T. and N.H.; visualization, I.P.; funding acquisition, I.P. All authors have read and agreed to the published version of the manuscript.

**Funding:** This research was funded by Japan Society for the Promotion of Science (JSPS) Grant-in-Aid for Early-career Scientists (JP20K15214).

**Data Availability Statement:** The data presented in this study are available on request from the corresponding author.

**Conflicts of Interest:** The authors declare no conflict of interest.

#### References

1. Hodgkinson, J.H.; Smith, M.H. Climate Change and Sustainability as Drivers for the next Mining and Metals Boom: The Need for Climate-Smart Mining and Recycling. *Resour. Policy* **2018**, *74*, 101205. [CrossRef]
2. Miah, M.D.; Kabir, M.H.; Koike, M.; Akther, S. Major Climate-Change Issues Covered by the Daily Newspapers of Bangladesh. *Environmentalist* **2011**, *31*, 67–73. [CrossRef]
3. Tabelin, C.B.; Yoo, K.; Li, J. Editorial for Special Issue “Novel and Emerging Strategies for Sustainable Mine Tailings and Acid Mine Drainage Management. *Minerals* **2021**, *11*, 902. [CrossRef]
4. World Meteorological Organization (WMO). *State of the Global Climate 2020*; WMO: Geneva, Switzerland, 2020; pp. 1–38.
5. The Paris Agreement. Available online: <https://unfccc.int/process-and-meetings/the-paris-agreement/the-paris-agreement> (accessed on 1 November 2021).
6. United Nations Goal 13 | Department of Economic and Social Affairs. Available online: <https://sdgs.un.org/goals/goal13> (accessed on 1 November 2021).
7. Tabelin, C.B.; Park, I.; Phengsaart, T.; Jeon, S.; Villacorte-Tabelin, M.; Alonzo, D.; Yoo, K.; Ito, M.; Hiroyoshi, N. Copper and Critical Metals Production from Porphyry Ores and E-Wastes: A Review of Resource Availability, Processing/Recycling Challenges, Socio-Environmental Aspects, and Sustainability Issues. *Resour. Conserv. Recycl.* **2021**, *170*, 105610. [CrossRef]
8. Hund, K.; La Porta, D.; Fabregas, T.P.; Laing, T.; Drexhage, J. *Minerals for Climate Action: The Mineral Intensity of the Clean Energy Transition*; The World Bank: Washington, DC, USA, 2020.
9. Tabelin, C.B.; Dallas, J.; Casanova, S.; Pelech, T.; Bournival, G.; Saydam, S.; Canbulat, I. Towards a Low-Carbon Society: A Review of Lithium Resource Availability, Challenges and Innovations in Mining, Extraction and Recycling, and Future Perspectives. *Miner. Eng.* **2021**, *163*, 106743. [CrossRef]
10. Alves Dias, P.; Bobba, S.; Carrara, S.; Plazzotta, B. *The Role of Rare Earth Elements in Wind Energy and Electric Mobility*; European Commission: Luxembourg, 2020.

11. Yoon, H.-S.; Kim, C.-J.; Chung, K.W.; Jeon, S.; Park, I.; Yoo, K.; Jha, M.K. The Effect of Grinding and Roasting Conditions on the Selective Leaching of Nd and Dy from NdFeB Magnet Scraps. *Metals* **2015**, *5*, 1306–1314. [CrossRef]
12. Choubey, P.K.; Singh, N.; Panda, R.; Jyothi, R.K.; Yoo, K.; Park, I.; Jha, M.K. Development of Hydrometallurgical Process for Recovery of Rare Earth Metals (Nd, Pr, and Dy) from Nd-Fe-B Magnets. *Metals* **2021**, *11*, 1987. [CrossRef]
13. Ballinger, B.; Schmeda-Lopez, D.; Kefford, B.; Parkinson, B.; Stringer, M.; Greig, C.; Smart, S. The Vulnerability of Electric-Vehicle and Wind-Turbine Supply Chains to the Supply of Rare-Earth Elements in a 2-Degree Scenario. *Sustain. Prod. Consum.* **2020**, *22*, 68–76. [CrossRef]
14. Alonso, E.; Wallington, T.; Sherman, A.; Everson, M.; Field, F.; Roth, R.; Kirchain, R. An Assessment of the Rare Earth Element Content of Conventional and Electric Vehicles. *SAE Int. J. Mater. Manuf.* **2012**, *5*, 473–477. [CrossRef]
15. Barteková, E. Chapter 10—The Role of Rare Earth Supply Risk in Low-Carbon Technology Innovation. In *Rare Earths Industry: Technological, Economic, and Environmental Implications*; de Lima, I.B., Filho, W.L., Eds.; Elsevier: Boston, MA, USA, 2016; pp. 153–169. ISBN 978-0-12-802328-0.
16. Jordens, A.; Cheng, Y.P.; Waters, K.E. A Review of the Beneficiation of Rare Earth Element Bearing Minerals. *Miner. Eng.* **2013**, *41*, 97–114. [CrossRef]
17. Garside, M. Rare Earth Mining—Global Distribution by Country 2020. Available online: <https://www.statista.com/statistics/270277/mining-of-rare-earths-by-country/> (accessed on 27 August 2021).
18. Muff, R.; Tamiraa, A. *Rare Earths of Mongolia: Evaluation of Market Opportunities for the Principal Deposits of Mongolia*; Ulaanbaatar/Bundesanstalt für Geowissenschaften und Rohstoffe: Hannover, Germany, 2013; p. 31.
19. Gerel, O.; Majigsuren, Y.; Munkhtsengel, B. Rare Earth Mineral Deposits. In *Mineral Resources of Mongolia*; Gerel, O., Pirajno, F., Batkhishig, B., Dostal, J., Eds.; Modern Approaches in Solid Earth Sciences; Springer: Singapore, 2021; pp. 185–210. ISBN 9789811559433.
20. Gronen, L.H.; Sindern, S.; Katzmarzyk, J.L.; Bormann, U.; Hellmann, A.; Wotruba, H.; Meyer, F.M. Mineralogical and Chemical Characterization of Zr-REE-Nb Ores from Khalzan Buregtei (Mongolia)—Approaches to More Efficient Extraction of Rare Metals from Alkaline Granitoids. *Minerals* **2019**, *9*, 217. [CrossRef]
21. Kempe, U.; Möckel, R.; Graupner, T.; Kynicky, J.; Dombon, E. The Genesis of Zr-Nb-REE Mineralisation at Khalzan Buregtei (Western Mongolia) Reconsidered. *Ore Geol. Rev.* **2015**, *64*, 602–625. [CrossRef]
22. Long, K.R. *The Future of Rare Earth Elements—Will These High-Tech Industry Elements Continue in Short Supply?* U.S. Geological Survey: Reston, VA, USA, 2011; pp. 1–43.
23. Rybak, A.; Rybak, A. Characteristics of Some Selected Methods of Rare Earth Elements Recovery from Coal Fly Ashes. *Metals* **2021**, *11*, 142. [CrossRef]
24. Goode, J.R. Rare Earth Elements. In *SME Mineral Processing & Extractive Metallurgy Handbook*; Society for Mining, Metallurgy & Exploration (SME): Englewood, CO, USA, 2019; Volume 2, pp. 1891–1916.
25. Abaka-Wood, G.B.; Zanin, M.; Addai-Mensah, J.; Skinner, W. Recovery of Rare Earth Elements Minerals from Iron Oxide-Silicate Rich Tailings—Part 1: Magnetic Separation. *Miner. Eng.* **2019**, *136*, 50–61. [CrossRef]
26. Kovalenko, V.I.; Tsaryeva, G.M.; Goreglyad, A.V.; Yarmolyuk, V.V.; Troitsky, V.A.; Hervig, R.L.; Farmer, G.L. The Peralkaline Granite-Related Khalzan-Buregtey Rare Metal (Zr, Nb, REE) Deposit, Western Mongolia. *Econ. Geol.* **1995**, *90*, 530–547. [CrossRef]
27. Wills, B.A.; Finch, J.A. Magnetic and Electrical Separation. In *Wills' Mineral Processing Technology*; Butterworth Heinemann: Oxford, UK, 2016; pp. 381–408.
28. Hanchar, J.M.; van Westrenen, W. Rare Earth Element Behavior in Zircon-Melt Systems. *Elements* **2007**, *3*, 37–42. [CrossRef]
29. Burnham, A.D. Key Concepts in Interpreting the Concentrations of the Rare Earth Elements in Zircon. *Chem. Geol.* **2020**, *551*, 119765. [CrossRef]
30. Jeon, S.; Ito, M.; Tabelin, C.B.; Pongsumrankul, R.; Tanaka, S.; Kitajima, N.; Saito, A.; Park, I.; Hiroyoshi, N. A Physical Separation Scheme to Improve Ammonium Thiosulfate Leaching of Gold by Separation of Base Metals in Crushed Mobile Phones. *Miner. Eng.* **2019**, *138*, 168–177. [CrossRef]
31. Tabelin, C.B.; Resabal, V.J.T.; Park, I.; Villanueva, M.G.B.; Choi, S.; Ebio, R.; Cabural, P.J.; Villacorte-Tabelin, M.; Orbecido, A.; Alorro, R.D.; et al. Repurposing of Aluminum Scrap into Magnetic Al<sup>0</sup>/ZVI Bimetallic Materials: Two-Stage Mechanical-Chemical Synthesis and Characterization of Products. *J. Clean. Prod.* **2021**, *317*, 128285. [CrossRef]
32. Choi, S.; Jeon, S.; Park, I.; Ito, M.; Hiroyoshi, N. Addition of Fe<sub>3</sub>O<sub>4</sub> as Electron Mediator for Enhanced Cementation of Cd<sup>2+</sup> and Zn<sup>2+</sup> on Aluminum Powder from Sulfate Solutions and Magnetic Separation to Concentrate Cemented Metals from Cementation Products. *J. Environ. Chem. Eng.* **2021**, *9*, 106699. [CrossRef]
33. Svoboda, J. *Magnetic Methods for the Treatment of Minerals*; Elsevier: Amsterdam, The Netherlands, 1987; pp. 1–235.
34. Jordens, A.; Marion, C.; Langlois, R.; Grammatikopoulos, T.; Rowson, N.A.; Waters, K.E. Beneficiation of the Nechalacho Rare Earth Deposit. Part 1: Gravity and Magnetic Separation. *Miner. Eng.* **2016**, *99*, 111–122. [CrossRef]
35. Rasool, R.; Lieberwirth, H. A Continuum Based Numerical Modelling Approach for the Simulation of WHIMS. *Miner. Eng.* **2018**, *118*, 97–105. [CrossRef]

- 
36. Jordens, A.; Sheridan, R.S.; Rowson, N.A.; Waters, K.E. Processing a Rare Earth Mineral Deposit Using Gravity and Magnetic Separation. *Miner. Eng.* **2014**, *62*, 9–18. [[CrossRef](#)]
  37. Hrouda, F.; Chlupacova, M.; Chadima, M. *The Use of Magnetic Susceptibility of Rocks in Geological Exploration*; Terraplius: Brno, Czech Republic, 2009; pp. 1–27.